Polymer Grafting of Graphene Oxide Through Esterification of Terephthalic Acid and Allyl Alcohol for Metronidazole Drug Delivery: Central Composite Design Optimization Study

Niloufar Torabi Fard
Islamic Azad University
Fariba Tadayon (f_tadayon@iau-tnb.ac.ir)
Islamic Azad University
Homayon Ahmad Panahi
Islamic Azad University
Elham Moniri
Islamic Azad University

Research Article

Keywords: Drug delivery, Graphene oxide, Polymer, Central composite design, Metronidazole

Posted Date: September 22nd, 2021

DOI: https://doi.org/10.21203/rs.3.rs-890332/v1

Polymer Grafting of Graphene Oxide through Esterification of Terephthalic Acid and Allyl Alcohol for Metronidazole Drug Delivery: Central Composite Design Optimization Study

Niloufar Torabi Fard [a], Fariba Tadayon [a,*], Homayon Ahmad Panahi [b], Elham Moniri [c]

[a] Department of Chemistry, North Tehran Branch, Islamic Azad University, Tehran, Iran

[b] Department of Chemistry, Central Tehran Branch, Islamic Azad University, Tehran, Iran

[c] Department of Chemistry, Varamin (Pishva) Branch, Islamic Azad University, Varamin, Iran

*Corresponding author: F_tadayon@iau-tnb.ac.ir

Abbreviations

Terephthalic acid	TPA
Allyl alcohol	AA
Graphene oxide	GO
P-toluene sulfonic acid	PTSA
2, 2'-azobisisobutyronitrile	AIBN
Metronidazole	MNZ
Fourier transform infrared spectroscopy	FTIR
Scanning electron microscopy	SEM
Energy dispersive X-ray spectrometry	EDX
Brunauer-Emmett-Teller	BET
X-ray diffractometer	XRD
Thermal gravimetric analysis	TGA
Response surface methodology	RSM
Central composite design	CCD
Nanoparticles	NPs
Taguchi design	TD
Full factorial design	FFD
Box-Behnken design	BBD
Plackett–Burman design	PBD
Barrett-Joyner- Halenda	BJH
Design Expert	DE
Polytetrafluoroethylene	PTFE
Dubinin-Radushkevich	D-R
Pseudo-first-order	PFO
Pseudo-second-order	PSO
Intra particle diffusion	IPD
Analysis of variance	ANOVA
Lack-of-fit	LOF
Standard deviation	SD
Coefficient of variation	CV
Two-dimensional	2D
Three-dimensional	3D

Abstract

The present study examined the direct esterification of terephthalic acid (TPA) with allyl alcohol (AA) on the graphene oxide (GO) surface in the presence of p-toluene sulfonic acid (PTSA) catalyst. Then, the surface of GO-TPAA was modified through polymerization reaction with 2,2'-azobisisobutyronitrile (AIBN) as a reaction initiator. The developed polymer was tested successfully as a nanocarrier for the metronidazole (MNZ) drug delivery. The resulting polymer was characterized by Fourier-transform infrared spectroscopy (FTIR), scanning electron microscopy (SEM), energy dispersive X-Ray (EDX), Brunauer-Emmett-Teller (BET), X-ray diffraction (XRD), and thermogravimetric analysis (TGA). The parameters were optimized by response surface methodology (RSM) based on the central composite design (CCD) experimental design. The maximum adsorption (93.31%) was obtained at pH=5, contact time of 15 min, and MNZ concentration of 15 mg L^{-1}. Analysis of variance (ANOVA) study proposed that the obtained equation for the adsorption of the MNZ is quadratic and it is significant for the model. The drug release behavior indicated that the amount of MNZ release from nanocarrier was significantly pH dependent. The released data were fitted into different kinetic release model equations for determining the best-fit release model for the nanocarrier. The adsorption kinetic data best fitted the pseudo-second-order model with a coefficient of determination (R^2) of 0.9999. The adsorption process was endothermic, following the Langmuir isotherm model (R^2=0.9956). MNZ release was studied in vitro using stimulated gastric fluid and stimulated intestinal fluid. The proposed nanoadsorbent can be useful for the rapid and efficient adsorption of the drug.

Keywords: Drug delivery, Graphene oxide, Polymer, Central composite design, Metronidazole

1 Introduction

Antibiotics are one of the most important types of antibacterial agent widely used in the prevention infectious of diseases. Since antibiotics are not biodegradable, most of these drugs are excreted into the environment [1, 2].

Metronidazole (MNZ) ($C_6H_9N_3O_3$, 171.15 g mol^{-1}), [1-(2 Hydroxyethyl)-2-methyl-5-nitroimidazole] is a kind of nitroimidazole antibiotic with strong anti-anaerobic activity, which is commonly used for treatment of the infections caused by anaerobic parasitic protozoa. MNZ drug has possible toxicological effects, including carcinogenic and mutagenic properties. Also,

it has been found to cause undesired side effects such as peripheral neuropathy, cerebellar dysfunction, gait disturbance, dysarthria, seizures, or encephalopathy [3, 4].

Drug delivery systems have been intensely investigated to improve the drug efficiency, to reduce dosing frequency, and to minimize drug side effects [5]. There are various controlled release drug carrier excipients used over the last few years such as metal nanoparticles (NPs) [6], polymers [7, 8], dendrimers [9], liposome [10], etc. Some researchers have proved that polymers are a significant drug carrier for delivering several types of antibiotic drugs [11-13]. Over the last few decades, carbon-based materials, for example, graphene [14-17], carbon nanotubes [18], graphitic carbon nitride [19], fullerene [20], and graphene foam [21] have been widely used.

Also, polymers have widely been used as biomaterials due to their favorable advantages such as biocompatibility, variety of structures and interesting bio-mimetic characteristics, easy design and preparation especially regarding controlled drug delivery [22].

Graphene oxide (GO), as an amphiphilic sheet has a large number of oxygen-containing functional groups. Chemical and thermal stability, good biocompatibility, low cost, and high surface area are the benefits of GO for drug delivery systems. Many researchers have revealed that GO derivatives have a high loading capacity of aromatic containing drugs [25, 26].

Esterification is a fundamental transformation of functional groups and is routinely used in industry and laboratories. Esterification of alcohols with carboxylic acids plays an essential role in the production of organic esters. The conventional catalysts for the esterification reaction generally include solid acid (resins and heteropoly acids) and inorganic acids (HCl, H_2SO_4 and H_3PO_4) [27, 28].

Response surface methodology (RSM), a set of statistical and mathematical methods, is a useful technique to achieve optimal conditions through the available resources [29]. The available experimental designs for procedure optimization include the following: CCD, Taguchi design (TD), full factorial design (FFD), Box-Behnken design (BBD), and Plackett–Burman design (PBD) [30]. Among these, the CCD has been widely applied in optimizing adsorption factors. CCD can fit a quadratic response with a minimum number of runs and analyze the interaction between the different factors, as well as help to optimize the responsive factors [31].

In this study, an efficient method was proposed to prepare GO/TPAA cl-poly (AA)/TPA. The GO/TPAA was synthesized via esterification of TPA and AA. The characterization of fabricated polymer was investigated using FTIR, SEM, EDX, BET, X-ray XRD, and TGA. Polymerization of GO/TPAA was done as a novel nanocarrier in MNZ

delivery. The drug loading efficiency and ability to control the release of the loaded drug of the MNZ/GO/TPAA cl-poly (AA)/TPA were examined. The concentration of MNZ, pH, and contact time were optimized using CCD for the adsorption of drug via the synthesized adsorbent. The sorption properties of the nanocarrier, such as adsorption isotherms, kinetics, and thermodynamics were also evaluated. The stimulated gastric fluid and stimulated intestinal fluid were used to assess the MNZ release in vitro. In addition, the reusability and the sorption mechanism of the polymers were investigated.

2 Materials and methods

2.1 Chemicals

MNZ with a purity of 99% was kindly donated by Kimyagaran Company (Tehran, Iran). Natural graphite powder was supplied by Sigma-Aldrich Co., Ltd (St. Louis, MO, USA). Terephthalic acid (TPA, $C_8H_6O_4$, 98%), p-toluene sulfonic acid (PTSA, $C_7H_8O_3S$, 98.5%), allyl alcohol (AA, C_3H_6O, 99%), and 2, 2'-azobisisobutyronitrile (AIBN, $C_8H_{12}N_4$, 98%) were procured from Merck Co., Ltd (Darmstadt, Germany). All chemicals used were of analytical reagent grade and used as received without any further purification. Also, high-quality distilled water produced by Milli-Q was used throughout this work. MNZ stock standard solution of 100 mg L^{-1} was prepared in double-distilled water and stored in a refrigerator (4°C). Cellulose dialysis membrane (MWCO; 12000 Da) was purchased from Sigma-Aldrich.

2.2 Characterization

The functional group of nanoparticles was identified within the range of 4000-400cm^{-1} via FTIR (PerkinElmer, Frontier, USA). Thermal gravimetric analysis for the nanoadsorbent was performed via a thermal analysis instrument (TGA, STA 1500, Rheometric scientific, Switzerland) under air atmosphere with a heating rate of 10°C min^{-1} from 25 to 600 °C. The morphology of adsorbent was examined using SEM (TESCAN MIRA3) equipped with an EDX at 20 kV acceleration voltage. The XRD analysis was carried out to identify the crystallinity of polymer using an X'pert PRO X-ray diffractometer with Cu-Ka radiation (PANalytical B.V., Netherlands). The specific surface area and the pore size distribution were measured by BET and Barrett-Joyner- Halenda (BJH) techniques, respectively. The total content of MNZ in the samples was estimated by UV–Vis spectrophotometer (Alignment, Cary 100).

2.3 Polymer preparation

2.3.1 Synthesis of graphene oxide nanosheets

GO was synthesized according to Hummers' method with modification [32]. Specifically, in a 100 mL round-bottom flask, 5 g of graphite powder and 5 g of $NaNO_3$ were dissolved into H_2SO_4 (230 mL) solution at room temperature using a mechanical stirrer. Then, 30 g of $KMnO_4$ was added to the above solution. The temperature was kept at 0 °C using an ice bath. After stirring the solution for 2 h, 460 mL of distilled water was poured into the above reaction solution. Further, 325 mL of H_2O_2 solution (30 %) was added dropwise to the previous solution under stirring during 2 h. Thereafter, the above solution was diluted in HCl (0.1 M). The obtained GO was filtered and dried at 45 °C under vacuum overnight.

2.3.2 Esterification of graphene oxide (GO/TPAA)

TPA and AA were attached on the surface of GO through esterification with the help of PTSA used as a catalyst. The general synthesis of the GO/TPAA was as follows: in the first step, a mixture of TPA (1 g) and GO (1 g) in 100 mL of ethanol was added to a 250 mL round-bottom flask with a magnetic stirrer. Then, 0.07 g PTSA as the catalyst was added and the solution was refluxed at 60 ºC. The reaction mixture was prepared for 6 h. Subsequently, the obtained precipitates were washed with double-distilled water in order to remove the remaining unreacted compounds. Finally, the products were dried in an oven with a temperature of 60 ºC for 6 h. In the second step, the hydroxyl groups were grafted on the surface with AA. Briefly, 0.7 g of precipitate, 0.06 g PTSA, and 10 mL AA were added into 30 mL of methanol. Thereafter, these components were refluxed at 60 °C for 6 h. After esterification, the resulting product was dried at room temperature.

2.3.3 Polymer grafting onto GO/TPAA (GO/TPAA Cl-Poly (AA) / TPA)

The organic phase, including 0.05 g of AIBN as initiator of polymerization and 0.5 g of GO/TPAA was mixed with the aqueous phase comprising 10 mL AA in 40 mL of ethanol. The polymerization was conducted under a nitrogen atmosphere at 70 °C. After refluxing the solution for 7 h, the resulting solution was collected through centrifugation, washed with ethanol and dried. Next, for specific adsorbent-drug interaction, 1 g TPA, 0.5 g GO/TPAA cl-poly (AA), 100 mL ethanol, and 0.07 g PTSA were added into 250 mL balloon-flask and refluxed for 6 h. At the end of the reaction, the mixture was centrifuged for 15 min at 4000 rpm. The resultant was dried for further experiments. Fig. 1 displays the preparation of GO/TPAA cl-poly (AA)/TPA.

Fig.1. Schematic representation of preparation of GO/TPAA cl-poly (AA)/TPA.

2.4 Adsorption experiments

In batch sorption tests, 0.01 g GO/TPAA cl-poly (AA)/TPA was mixed with 25 mL aqueous solutions with the concentration range between 5 to 80 mg L^{-1}. The pH value of the solutions was adjusted to 3-9 by a magic buffer solution (acetic acid 0.05 mol L^{-1}, phosphoric acid 0.06 mol L^{-1}, boric acid 0.04 mol L^{-1} and sodium hydroxide 2 mol L^{-1}). To examine the effect of temperature on MNZ sorption, the experimental temperatures were adjusted to 20-50 °C, and the mixture was stirred for 15 min at 450 rpm. After stirring, the reaction mixture was placed into a centrifuge tube. Then, the centrifuge was performed at 5000 rpm. Afterward, the drug content was measured by UV–Vis spectrophotometer at 316 nm. The sorption capacity of the MNZ for GO/TPAA cl-poly (AA)/TPA was calculated using the following formula:

$$q_e = (C_0 - C_e)\, V/M \quad (1)$$

Here, q_e represents the sorption capacity (mg g^{-1}), C_0 and C_e denote the initial and equilibrium MNZ concentration in the solutions (mg L^{-1}), V shows the volume solution (L), and M is the weight of GO/TPAA cl-poly (AA)/TPA (g).

2.5 Loading and release of MNZ onto the GO/TPAA Cl-Poly (AA)

Initially, 0.1 g of GO/TPAA cl-poly (AA)/TPA was mixed with 25 mL of MNZ solution with concentration of 50 mg L^{-1}.After stirring for 30 min at 25 °C, the mixture was transferred into a centrifugation tube and centrifuged for 10 min at 4000 rpm. Subsequently, the concentration of free MNZ in the supernatant was measured through UV–Vis spectroscopy at 316 nm. Thereafter, the nanoadsorbent was dried to obtain the drug loaded polymer. The sample prepared by this method was named MNZ/GO/TPAA cl-poly (AA)/TPA. The in vitro release of MNZ from MNZ/GO/TPAA cl-poly (AA)/TPA was conducted according to the following process. Initially, 0.1 g of MNZ-loaded GO/TPAA cl-poly (AA)/TPA, which was incubated in a dialysis sac was suspended in 50mL of phosphate-buffered saline (PBS; pH = 7.4 and 1.2) at 37 °C. Then, at different selected time intervals: 0.5, 1, 1.5, 2, 2.5, 3, 3.5, 4, 4.5, 5, 5.5 and 6 h, 3 mL of the release media was withdrawn and replaced with fresh media. Finally, the amount of MNZ released from the MNZ/GO/TPAA cl-poly (AA)/TPA was analyzed via UV–Vis spectroscopy (λ_{max}= 316 nm).

2.6 Design of experiments using central composite design

CCD was performed for the design of experiments (COD) between three independent factors, including pH (A), contact time (B), and the concentration of MNZ (C) by Design Expert 12.0 (DX) software. These factors were considered at five different levels coded as –α, −1, 0, +1, and +α (Table.1). Based pm Eq (2), 20 experiments were designed.

$$N = 2^f + 2f + C_0 \quad (2)$$

Where f and C_0 are the number of variables and replicates in center point, respectively. Experiments incorporating eight factorial points, six axial points, and six replicate at the center were suggested by the software (Table 2). The response of variables was determined using a quadratic model (Eq 3).

$$Y = \beta_0 + \sum_{i=1}^{k} \beta_i X_i + \sum_{i=1}^{k} \beta_{ii} {X_i}^2 + \sum_{i=1}^{k} \sum_{i \neq j=1}^{k} \beta_{ij} X_i X_j + \varepsilon \quad (3)$$

Where, Y denotes the predicted response, β_o shows the constant coefficients, β_i, β_{ii} and β_{ij} represent the regression coefficients for the linear, quadratic, and interaction terms, respectively. X_i and X_j are the coded values of the factors, respectively. K expresses the number of the independent factors.

Table 1. Experimental variables and their levels in CCD.

Variables	Code	Unit	Coded variable levels				
			- α	**-1**	**0**	**+1**	**+ α**
pH	A	---	3	4	5	6	7
Contact time	B	min	5	10	15	20	25
Concentration	C	mg L^{-1}	5	10	15	20	25

2.7 Adsorption isotherms, kinetics, and thermodynamics

2.7.1 Isotherm studies

Adsorption isotherm studies were performed by GO/TPAA cl-poly (AA)/TPA for different concentrations of MNZ in the range of 5 to 80 mg L^{-1} at optimum pH. After the equilibrium

time, the supernatant was filtered by a polytetrafluoroethylene (PTFE) syringe filter (0.22 μm, Chromafil, Germany). Next, the concentration of the clear supernatant was measured by a UV–Vis spectrophotometer. Meanwhile, the isotherm studies were investigated at various temperatures (298.15, 308.15 and 323.15 K). In our research, four adsorption isotherm models (Langmuir [33], Freundlich [34], Temkin [35] and Dubinin-Radushkevich (D-R) [36]) were used to fit the equilibrium data of MNZ on GO/TPAA cl-poly (AA)/TPA. The linear form of the selected models can be presented using the following equation:

$$Ce/qe = 1/kl.qmax + Ce/qmax \quad (4)$$

$$ln\, qe = ln\, Kf + 1/n\, ln\, Ce \quad (5)$$

$$qe = B\, lnCe + B\, lnKT \quad (6)$$

$$lnqe = ln\, qs - D\varepsilon 2 \quad (7)$$

Where, C_e (mg L^{-1}) refers to the concentration of MNZ at equilibrium, q_e and q_{max} (mg g^{-1}) represent the equilibrium and maximum monolayer sorption capacity, respectively. K_l, K_f and K_t denote the Langmuir, Freundlich, and Temkin equilibrium constants, respectively. Also, B=RT/b is the heat of adsorption (J mol^{-1}), R (8.314 J mol^{-1} K^{-1}), T (K) and b represent the universal gas constant, the adsorption temperature and the Temkin isotherm constant, respectively. D (mol^2 kJ^{-2}) and ε show the constant of the adsorption energy and the Polanyi potential.

2.7.2 Kinetic studies

The rate of MNZ adsorption onto GO/TPAA cl-poly (AA)/TPA was examined within the contact time range from 2 to 60 min. Also, the kinetic behavior of MNZ was obtained at pH=5. Three kinetic models (pseudo-first-order model (PFO) [37], pseudo-second-order model (PSO) [38] and the intraparticle diffusion (IPD) [39] model) were used to consider the mechanism of the adsorption of MNZ onto the GO/TPAA cl-poly (AA)/TPA. The linear form of the selected models can be expressed as follows:

$$Log\,(q\,e - q\,t) = Log\,q\,e - k1\,t\,/\,2.303 \quad (8)$$

$$t\,/\,q\,t = 1\,/k2\,q\,e2 + t\,/q\,e \quad (9)$$

$$q\,t = Ki\,t\,1/2 + Ci \quad (10)$$

Where, q_t (mg g^{-1}) represents the adsorption capacity of GO/TPAA cl-poly (AA)/TPA per unit of time. k_1 (min^{-1}), k_2 (g mg^{-1} min^{-1}) and k_i (mg g^{-1} min^{-1}) are the adsorption rate constant of the PFO, PSO, and IPD kinetic model, respectively. T (min) denotes t the adsorption time. C_i is the thickness of the boundary layer.

2.7.3 Thermodynamic studies

To explore thermodynamic parameters, similar experimental conditions were carried out at different temperatures (298.15, 308.15 and 323.15 K). The enthalpy change (ΔH^o; J mol^{-1}), the Gibbs free energy (ΔG^o; J mol^{-1}), and the entropy change (ΔS^o; J mol^{-1} K^{-1}) were calculated to inspect the influence of rising temperatures on the adsorption of MNZ onto GO/TPAA cl-poly (AA)/TPA.

$$K\,d\ =\ q\,e/Ce \tag{11}$$

$$ln\,K\,d\ =\ -\,\Delta Ho\ /\ RT\ \ +\ \Delta So\ /R \tag{12}$$

$$\Delta Go\ =\ \Delta Ho\ -\ T\ \Delta So \tag{13}$$

Where, K_d, R ($J \cdot mol^{-1} \cdot K^{-1}$) and T (K) represent the thermodynamic equilibrium constant, the gas constant, and temperature, respectively.

3 Results and discussion

3.1 Characterization

3.1.1 SEM and EDX analysis

The surface morphologies of GO/TPAA, GO/TPAA cl-poly (AA), and GO/TPAA cl-poly (AA)/TPA with various magnifications are shown in Fig. 2. The GO/TPAA NPs had a far rougher, thicker and uneven surface, implying the aggregation of many small ester groups on the surface of GO (Fig. 2a). The particle size of the GO/TPAA NPs was smaller than 55.15 nm. As can be seen in Fig. 2b, polymer grafting on the GO/TPAA surface has induced some morphological variations which have also been presented in this section. After polymerization, the NPs size increased considerably. In comparison with the GO/TPAA cl-poly (AA), GO/TPAA cl-poly (AA)/TPA indicates a rougher surface with some wrinkles because of the TPA coating on the polymer surface (Fig. 2c). In other words, the crumpled GO/TPAA cl-poly (AA)/TPA is related to abundant oxygen-containing functional groups such as carbonyl,

hydroxyl, and carboxyl on the polymer layers. Also, elemental compositions of GO/TPAA, GO/TPAA cl-poly (AA), and GO/TPAA cl-poly (AA)/TPA were identified by EDX analysis. In EDX spectra of GO/TPAA (Fig. 2a), the weight percentage of GO/TPAA was 70.06%, 29%, and 0.4% for C, O, and S, respectively. There is no evidence for nitrogen atoms in GO/TPAA NPs. Following surface polymerization, the weight percentage of C, S, and N increased, while the atomic weight ratio of O decreased (Fig.2b). Further, in EDX spectra of GO/TPAA cl-poly (AA)/TPA (Fig. 2c), the O, N and S contents were significantly reduced. On the other hand, the peak intensity of C in the spectra of GO/TPAA cl-poly (AA)/TPA increased. Overall, the presence of Au atom is due to gold spray treatment of the NPs.

Fig.2. SEM and EDX images of (a) GO/TPAA, (b) GO/TPAA cl-poly (AA), and (c) GO/TPAA cl-poly (AA)/TPA.

3.1.2 Thermo-Gravimetric analysis

The thermal behavior of GO/TPAA cl-poly (AA)/TPA polymer was analyzed by the TGA analysis. The TGA curve of the GO/TPAA cl-poly (AA)/TPA polymer is displayed in Fig.S1. The first mass loss from 100 to 250 °C was attributed to the surface grafting of GO/TPAA with polymer. The second stage of mass loss from 250 to 600 °C was attributed to the degradation of the backbone GO. In other words, 10.71 % of the weight loss was related to the modification of the GO/TPAA by polymer and 73.6 % was associated with the degradation of the carbon skeleton.

3.1.3 XRD analysis

The crystal structure of GO/TPAA cl-poly (AA)/TPA was determined by XRD spectra (Fig.S2). In the XRD pattern of GO/TPAA cl-poly (AA)/TPA, strong diffraction peaks were found at 12.12°, 17.50°, 25.37°, and 28.03°. Also, sharp and strong peaks at 17.50° and 28.03° occurred with 24050 and 32350 cts, respectively. The average crystallite size of GO/TPAA cl-poly (AA)/TPA was computed using Debye-Scherrer equation, which was 53.5 nm. The Debye-Scherrer equation can be expressed as follows:

$$D = 0.89\lambda / (\beta Cos\theta) \quad (14)$$

Where D, λ, β, and θ are the average size of nanoadsorbent, the X-ray wavelength (0.154 nm), the full width at half maximum (FWHM) in radiation and the angle of diffraction, respectively.

3.1.4 FT-IR analysis

The FTIR spectra of GO/TPAA and GO/TPAA cl-poly (AA)/TPA are shown in Fig.S3. Based on in Fig.S3a, the strong absorbance at 3431 cm^{-1} can be related to the O-H stretching vibration for carboxyl and hydroxyl. The characteristic absorption peaks at 2938, 1411, and 1286 cm^{-1} are assigned to the stretching vibrations of aliphatic C-H, CH_2, and C-O bands, respectively. Furthermore, the peaks at 1634 cm^{-1} are attributed to the out-of-plane stretching vibration of the OH group. The characteristic absorption band at 1679 cm^{-1} and the intensity at 1286 cm^{-1} increased simultaneously in GO/TPAA cl poly (AA)/TPA compared with GO/TPAA because of the OH stretching vibration and C-O bending vibrations. The shift in CH_2 stretching vibration also confirms the same (Fig.S3b). According to the results, the FT-IR spectra demonstrated the successful synthesis of GO/TPAA cl-poly (AA)/TPA.

3.1.5 Nitrogen adsorption

In this study, the nitrogen (N_2) adsorption-desorption isotherm (BET) and pores size distribution (BJH) parameters of GO/TPAA cl-poly (AA)/TPA were investigated. The N_2 adsorption-desorption isotherms of the GO/TPAA cl-poly (AA)/TPA are depicted in Fig.S4. The N_2 sorption isotherms are type IV isotherms with a distinct hysteresis loop at the relative pressure P/P_0 ranging from 0.5 to 0.8. The total pore volume was 0.014 $cm^3\ g^{-1}$, the BET surface area was 4.40 $m^2\ g^{-1}$, and the mean pore diameter of the nanoadsorbent was 13.62 nm. Also, a high BET surface area and nanoscale size indicate that GO/TPAA cl-poly (AA)/TPA can be favorable for MNZ sorption.

3.2 Optimization of parameters on the adsorption efficiency

The influence of pH on sorption of MNZ by GO/TPAA cl-poly (AA)/TPA was investigated within the pH range of 3 to 9. It was observed that the maximum adsorption capacity of GO/TPAA cl-poly (AA)/TPA was at pH of 5, and then diminished by increasing pH (Fig. 3a). The effect of pH_{PZC} (point of zero charge) in this experiment was studied within the range 3 to 10 (Fig. 3b). At pHs higher than 6, the surface of GO/TPAA cl-poly (AA)/TPA would be negatively charged, while the positive charges occur at pHs lower than 6. Accordingly, the pH_{PZC} value of GO/TPAA cl-poly (AA)/TPA was 6. Fig. 3c exhibits the effect of contact time

for the adsorption of MNZ by GO/TPAA cl-poly (AA)/TPA. The results indicated that the adsorption efficiency was enhanced by increasing contact time up to 15 min. It can be related to a large number of active sites. The highest adsorption efficiency was attained at 15 min, and there were no significant variations with longer contact times. In order to evaluate the influence of temperature on adsorption efficiency, different temperatures (25 to 50°C) for sorption MNZ by GO/TPAA cl-poly (AA)/TPA were studied at pH 5. As can be seen from the result in Fig. 3d, the adsorption efficiency decreased significantly when the temperature increased from 30 to 50 °C.

Fig.3. The influence of pH (a), pH $_{PZC}$ (b), contact time (c) and temperature (d) on the sorption of MNZ onto GO/TPAA cl-poly (AA)/TPA.

3.3 Results of central composite design

The experimental conditions for the maximum adsorption, including pH, contact time, and MNZ concentration were optimized using CCD and 20 experiments were obtained (Table 2). According to this table, each experiment row was accomplished under specific conditions and the adsorption percentage was calculated. The adsorption efficiency was in the range of 15.13% to 93.31% and the maximum adsorption percentage (experimental=94.63, predicted=93.31) is attributed to the pH=5, contact time of 15 min, and concentration of 15 mg L^{-1}.

Table 2. Experimental design and results of the CCD.

Run	A: pH	B: Time (min)	C: Concentration (mg L^{-1})	Adsorption (%)	
				Experimental	Predicted
1	5	15	15	91.65	93.31
2	5	15	15	93.58	93.31
3	4	20	20	73.23	76.80
4	6	20	10	63.21	66.95
5	4	10	10	60.67	63.65
6	6	10	20	52.12	56.70
7	4	20	10	70.00	70.41
8	5	15	15	92.95	93.31
9	4	10	20	63.54	64.79
10	6	10	10	58.87	60.29
11	5	15	15	94.52	93.31
12	6	20	20	66.60	68.61
13	5	15	25	80.00	75.07
14	5	25	15	89.65	85.56
15	5	15	5	75.76	72.26
16	7	15	15	20.23	15.13
17	5	15	15	94.12	93.31
18	5	15	15	94.63	93.31
19	5	5	15	71.23	66.89
20	3	15	15	30.00	26.67

3.4 Analysis of variance (ANOVA)

To investigate the validity of the CCD model, the impact of factors, as well as the interaction between them, ANOVA was performed (Table 3). The coefficients obtained from the ANOVA table were replaced in Eq (3), and it was changed to Eq (15).

$$R = 93.31 - 2.89A + 4.67B + 0.7012C - 0.0250AB - 1.18AC + 1.31BC - 18.10A2 - 4.27B2 - 4.91C2 \quad (15)$$

As can be seen in Table 3, the results of the quadratic model indicated that the pH and contact time possess remarkable effects on the adsorption efficiency of MNZ because their p-values were lower than 0.05. The F-value related to the model is equal to 189.17, as well as p-value< 0.0001 confirms that the created model is significant. Also, A^2, B^2, and C^2 are significant as p-values were < 0.05. In addition, the lack-of-fit (LOF) value has not been significant thus confirming the acceptability of the quadratic model. The predicted R^2 was 0.9688 and the adjusted R^2 of 0.9901 was in reasonable agreement with each other. In addition, the adequate precision (signal to noise ratio) of the model is far higher than 4. The ratio of 45.478 shows a suitable signal to noise ratio. In addition, a low standard deviation (SD) (2.22) and coefficient of variation (C.V) value (3.09) were attained, showing the model is suitable.

Fig.4 (a) demonstrates the correlation between externally studentized residuals and the normal probability of data. The closeness of the points to the straight line can be observed, indicating the normal distribution of residuals. In addition, the plot related to the externally studentized residuals values against predicted is studied (Fig.4b). The results indicated that the obtained residuals points were scattered near a zero line with the range between −4.59 to 4.59. The evaluation of the relationship between the predicted and actual values revealed that the points are on the straight line, and there is a strong closeness between predicted and experimental values (Fig.4c).

Fig. 4. (a) Normal plot of residuals, (b) plot of residuals versus predicted, and (c) plot of predicted values versus actual values related to the adsorption of the drug

Table 3. ANOVA of the adsorption efficiency for response quadratic model.

Source	Sum of Squares	df	Mean Square	F-value	p-value	
Block	87.28	2	43.64			
Model	8385.88	9	931.76	189.17	< 0.0001	**significant**
A-pH	133.29	1	133.29	27.06	0.0008	
B-Time	348.57	1	348.57	70.77	< 0.0001	
C-Concentration	7.87	1	7.87	1.60	0.2419	
AB	0.0050	1	0.0050	0.0010	0.9754	
AC	11.19	1	11.19	2.27	0.1702	
BC	13.78	1	13.78	2.80	0.1329	
A^2	7864.45	1	7864.45	1596.69	< 0.0001	
B^2	437.76	1	437.76	88.88	< 0.0001	
C^2	578.79	1	578.79	117.51	< 0.0001	
Residual	39.40	8	4.93			
Lack of Fit	36.18	5	7.24	6.73	0.0737	**not significant**
Pure Error	3.22	3	1.07			
Cor Total	8512.57	19				
R^2	0.9953					
Adjusted R^2	0.9901					
Predicted R^2	0.9688					
Adeq Precision	45.478					

3.5 Three-dimensional and two-dimensional response surface plots

In order to consider the interaction of different adsorption factors, the two-dimensional (2D) contour plot and three-dimensional (3D) diagram are illustrated in Fig.5. By increasing pH up to 5 and contact time up to 15 min, the adsorption efficiency was enhanced (Fig 5a). Fig. 5 (b) reveals that when the concentration diminished and the pH increased, the MNZ adsorption response declined. As indicated in Fig.5 (c), it was observed that the MNZ adsorption was improved by increasing the contact time and concentration, when the pH was fixed at 5.

Fig.5. Response surface and contour plots for the adsorption efficiency of MNZ: (a) pH and contact time; (b) pH and concentration; (c) time and concentration.

3.6 Adsorption isotherm studies

Adsorption isotherm studies were performed with the nanoadsorbent at various concentrations of MNZ (5 to 80 mg L^{-1}) at different temperatures (298.15, 308.15 and 323.15 K). Table S1 reports the adsorption isotherm parameters for adsorption of MNZ onto GO/TPAA cl-poly (AA)/TPA. According to the results, the maximum adsorption capacity (q_{max}) and K_L values increased with elevation of temperature. At all test temperatures, the obtained values of 1/n

were below one, indicating high adsorption density. Further, the K_f parameter values of the Freundlich model enhanced by increasing the temperature range of 298.15 to 323.15 K. It can be deduced that, the K_f values were 0.336 kJ mol^{-1}, 0.726 kJ mol^{-1}, and 1.351 kJ mol^{-1} for 298.15 K, 308.15 K, and 323.15 K, respectively. According to the results, the coefficient of determination (R^2) value of the Langmuir isotherm model was greater than that of the other isotherm models for the adsorption of MNZ. It would propose a monolayer sorption of the drug on the nanoadsorbent. The R_L was within the range of 0-1 which confirms desirable adsorption of MNZ from the aqueous solution. On the other hand, the q_e value of nanoadsorbent for MNZ increased by elevating the temperature. Also, the q_s values of the D-R models rose with the increase in the temperature range of 298.15 to 323.15K.

3.7 Adsorption kinetic studies

Three kinetic models, viz., PFO, PSO, and IPD models were carried out to examine the kinetics of the sorption method. Compared with the PFO and IPD models, PSO model appeared to well fit the experimental data given the higher R^2 values. The q_e (calculated) and q_e (experimental) of the PFO and PSO are presented in Table S2. The values of q_e related to the PSO model were close to the values of q_e (experimental). Thus, the PSO kinetic model is usually appropriate for the chemisorption procedure.

3.8 Adsorption thermodynamic studies

Experiments were performed at three different temperatures (298.15, 308.15, and 323.15 K) to determine the thermodynamic parameters (i.e., $\Delta H°$, $\Delta S°$, and $\Delta G°$). The values of $\Delta S°$ and $\Delta H°$ were obtained from the intercept and slope of the linear plots in Fig. S5, respectively. The obtained thermodynamic parameters are listed in Table S3. The positive $\Delta H°$ value suggested the endothermic nature of the sorption method of MNZ, and the sorption capacity increased as the temperature was elevated. The negative $\Delta G°$ values indicated the thermodynamic feasibility and spontaneity of the MNZ onto GO/TPAA cl-poly (AA)/TPA, and the diminishing $\Delta G°$ values showed a proper level of spontaneity as temperature increased from 298.15 to 323.15 K. Furthermore, the positive value of $\Delta S°$ indicated the degree of freedom of the adsorbed species increased during the adsorption process.

3.9 In-vitro drug release study and release kinetics

In vitro MNZ release profile from GO/TPAA cl-poly (AA)/TPA was performed in a stimulated intestinal fluid (PBS, pH=7.4) and stimulated gastric fluid (PBS, pH=1.2) for a period of 6 h as presented in Fig. 6. The slower release rate of MNZ in a stimulated intestinal fluid compared to the gastric fluid is also evidenced. The MNZ was rapidly released in a stimulated gastric fluid, where 49 % of the MNZ was released within 1 h and 98 % of the drug was released within the next 5 h. On the other hand, in the stimulated intestinal fluid 21 % was released within 1 h and 74 % of the drug was released within the next 5 h. Accordingly, more than 90 % of MNZ was released at pH of 1.2 and time of 6 h, while only about 74% of drug released at pH of 7.4. It is evident that the MNZ release of the nanocarrier is strongly pH-dependent.

The data obtained from the in vitro release studies of MNZ loaded PLGA NPs were fitted to different non-linear kinetic models such as zero order (Eq.16), first order (Eq.17), Korsmeyer-Peppas (Eq.18), and Higuchi (Eq.19) model to interpret the mechanism of MNZ release. The zero-order model may be utilized if the drug molecule does not disaggregate and release the drug very slowly. First-order kinetic model may describe the dissolution and swelling behavior of drug in a water-soluble matrix. The Higuchi kinetic model may be described if the drug molecules dispersed in a uniform medium behave as a dispersing medium. The distinct release phenomena involving either diffusion or swelling can be described by Korsmeyer-Peppas kinetic model [40-42]. The equations of the models are described as:

$$Q_t/Q_\infty = K_0 \times t \tag{16}$$

$$Q_t/Q_\infty = 1\text{-}e^{-K_1 \times t} \tag{17}$$

$$Q_t/Q_\infty = K_{KP} \times t^n \tag{18}$$

$$Q_t/Q_\infty = K_H \times t^{1/2} \tag{19}$$

Where, Q_t (%) denotes the percentage of drug dissolved at time t, Q_∞ (%) represents the total percentage of MNZ dissolved. The Q_t/Q_∞ shows the fraction of MNZ dissolved at time t. K_0 indicates the zero-order rate constant, K_1 reveals the first-order rate constant, K_{KP} reflects the Korsmeyer-Peppas rate constant, and K_H represents the Higuchi rate constant. n shows the diffusion constant. Generally, "n" has four probabilities, including n<0.5 (Fickian diffusion);

529 0.5< n< 0.9 (non-Fickian transport); n= 0.9 (case II transport); and n>0.9 (super case II
530 transport) [43]. The model with highest R^2 was deliberated to be the best fit model. According
531 to the results of Table S4, among the models fitted, zero-order model indicated the best R^2 at
532 pH=1.2. The MNZ release mechanism was investigated based on the "n" values in the
533 Korsmeyer-Peppas model. n=0.8 was obtained for R^2=0.9966, indicating that the release
534 mechanism was non-Fickian diffusion (pH=1.2). On the other hand, the MNZ release profile
535 at pH= 7.4 buffer was best fitted in the first-order kinetic model. Also, the MNZ release
536 mechanism in case of GO/TPAA cl-poly (AA)/TPA at pH=7.4 can be described as a non-
537 Fickian diffusion-controlled release (n=1, R^2= 0.983; super case II transport).
538
539 **Fig.6.** Drug release behavior in stimulated intestinal fluid and in stimulated gastric fluid.
540
541 **3.10 Reusability study**
542
543 To explore the reusability of GO/TPAA cl-poly (AA)/TPA, a certain amount of GO/TPAA cl-
544 poly (AA)/TPA was added into a 10 mL flask containing 1.5 mL MNZ solution, and then
545 stirred at room temperature for 15 min. After centrifugation at 4000 rpm for 15 min, the black
546 precipitate was collected and kept in methanol at 50 °C for 5 min. Subsequently, the mixture
547 was again centrifuged for 5 min. This procedure was repeated ten times to estimate the
548 reusability efficiency. As presented in Fig.S6, the recovery of GO/TPAA cl-poly (AA)/TPA
549 diminished from 100 % to 61 % after reusing for ten times. As can be seen in Fig.S6, it is clear
550 that the GO/TPAA cl-poly (AA)/TPA has lost its activity by about 60 % after the sixth cycle
551 of tests. It was found that the nanoadsorbent could be reused for six consecutive cycles.
552
553 **3.11 A comparison of the results of MNZ release using different nanocarriers**
554
555 For comparison, the releasing time of the MNZ among various nanocarriers was also evaluated.
556 As can be seen in Table 4, there is a highest MNZ release in comparison to the other
557 nanocarriers under similar conditions. Among the four nanocarriers, the release of MNZ is
558 rapid from the GO/TPAA cl-poly (AA)/TPA compared to other groups. As shown, the drug
559 release from the GO/TPAA cl-poly (AA)/TPA was sustained and continuously increased
560 throughout the entire experiment (74 %; 6 h) compared to other nanocarriers. These results
561 suggest that with the help of the polymer, the polymeric chain was opened and the ability of
562 the nanocarrier for MNZ sorption in aqueous solution was enhanced, which is due to the
563 increasing interactions between MNZ and functional groups of polymer.

564 **Table 4.** Comparison of different nanocarriers related to the MNZ release at pH 7.4

Nanocarrier	Drug release (%)	Time (h)	Ref.
Ploronic L101	>90	18	[44]
Chitosan–TPP	70	12	[45]
Metronidazole magnetic nanosuspension (MMNS)	80	7	[46]
Poly(ethylene glycol-colactide) (PELA)	60	160	[47]
GO/TPAA cl-poly (AA)/TPA	74	6	This study

565

566

567 **4 Conclusion**

568

569 In summary, functionalization of GO with polymer was achieved via esterification of TPA and
570 AA with p-TSA as a catalyst on the GO surface. The as-prepared polymer indicated attractive
571 features for the MNZ storage/release as a nanocarrier. Also, the structure of the as-prepared
572 nanocarrier was characterized using SEM/EDX, FTIR, XRD, TGA, and BET techniques. The
573 effects of three factors (pH, contact time and concentration) were studied using the RSM
574 technique based on the CCD. CCD results proposed the adsorption procedure to follow
575 quadratic equation. The kinetic data and sorption equilibrium best fitted the pseudo-second-
576 order kinetic and Langmuir models, respectively. Thermodynamic studies revealed that the
577 procedure was endothermic and spontaneous. The reusability of nanoadsorbent was explored
578 up to six cycles. The MNZ release curve of nanocarrier was examined in a stimulated intestinal
579 fluid (pH=7.4) and in a stimulated gastric fluid (pH=1.2) at 37 °C. MNZ was rapidly released
580 from the nanocarrier in a stimulated gastric fluid with approximately 98 %. The release kinetic
581 models indicated that the GO/TPAA cl-poly (AA)/TPA was found to be best fit zero–order and
582 first-order kinetic models at pH of 1.2 and 7.4, respectively. The results of release kinetic
583 studies revealed that the drug release from the GO/TPAA cl-poly (AA)/TPA occurred through
584 non-Fickian diffusion mechanism (pH=1.2 and 7.4).

585

586 **Acknowledgements**

587

588 The authors would like to acknowledge Islamic Azad University (North Tehran Branch) for
589 financial support of this work.

590

591 **Declaration of interest statement**

Conflict of Interest

No conflict of interest exists.

Funding

No funding was received for this work.

References

1. M. Malakootian, K. Karthik, M. Amiri Gharaghani, A. Dehdarirad, A. Nasiri, Y. Dadban Shahamat, H. Mahdizadeh, J. Environ. Chem. Eng 7, 103457 (2019).

2. M. Malakootian, M.H. Ehrampoush, H. Mahdizadeh, A. Olpayegani, J. Water. Chem. Techno 40, 327(2018).

3. Y. Xia, Q. Zhang, G. Li, X. Tu, Y. Zhou, X. Hu, J. Taiwan. Inst. Chem. E 96, 256 (2019)

4. Y. Yamamoto, N. Asai, A. Furuhashi, T. Ono, Y. Yamagishi, H. Mikamo, Y. Kazaoka, J. Infect. Chemother 25, 1057 (2019)

5. R. Grillo, F.V. Dias, S.M. Querobino, C. Alberto-Silva, L.F. Fraceto, E. de Paula, D.R. de Araujo, Colloid. Surface. B 174, 56(2019)

6. A. Simonazzi, A.G. Cid, M. Villegas, A.I. Romero, S.D. Palma, J.M. Bermu´dez, Drug Targeting and Stimuli Sensitive Drug Delivery Systems, 3rd edn. (Elsevier, 2018), pp.81-116

7. W.B. Liechty, D.R. Kryscio, B.V. Slaughter, N.A. Peppas, Annu. Rev. Chem. Biomol. Eng 1, 149 (2010)

8. N. Kamaly, B. Yameen, J. Wu, O.C. Farokhzad, Chem. Rev 116, 2602(2016)

9. A. Singh Chauhan, Molecules 23, 938 (2018)

10. V.M. Knepp, R.S. Hinz, F.C. Szoka Jr, R.H. Guy, J. Control. Release 5,211 (1987)

11. N.D. Stebbins, M.A. Ouimet, K.E. Uhrich, Adv. Drug. Deliver. Rev 77 (2014)

12. M.H. Xiong, Y. Bao, X.Z. Yang, Y.H. Zhu, J. Wang, Adv. Drug. Deliv. Rev 30, 63 (2014)

13. P. Gao, X. Nie, M. Zou, Y. Shi, G. Cheng, J. Antibiot 64, 625 (2011)

14. S. Kumar, S.D. Bukkitgar, S. Singh, V. Pratibha Singh, K.R. Reddy, N.P. Shetti, C. Venkata Reddy, V. Sadhu, S. Naveen, ChemistrySelect 4, 5322 (2019)

15. G. Manasa, R.J. Mascarenhas, A.K. Satpati, B.M. Basavaraja, S. Kumar, C Colloid Surface B 170, 144 (2018)

16. N.P. Shetti, S.J. Malode, D.S. Nayak, G.B. Bagihalli, K.R. Reddy, K. Ravindranadh, C.V. Reddy, Microchem. J 149, 103985 (2019)

17. S. Wang, L. Zhao, R. Xu, Y. Ma, L. Ma, J. Electroanal. Chem 853, 113527 (2019)

18. S. Nisha, A.S. Kumar, J. Electroanal. Chem 839, 214 (2019)

19. A. Mohammad, K. Ahmad, A. Qureshi, M. Tauqeer, S.M. Mobin, Sensor. Actuat. B-Chem 277, 467 (2018)

20. P.K. Brahman, N. Pandey, S.N. Topkaya, R. Singhai, Talanta 134,554 (2015)

21. H.Y. Yue, S.S. Song, X.R. Guo, S. Huang, X. Gao, Z. Wang, W.Q.Wang, H.J. Zhang, P.F.Wu, J. Electroanal. Chem 838,142 (2019)

22. D. Bennet, S. Kim, Application of Nanotechnology in Drug Delivery, 25th edn. (2014), pp. 257-310.

23. M. Pooresmaeil, H. Namazi, Mater. Chem. Phys 218, 62 (2018)

24. J. Liu, L. Cui, D. Losic, Acta. Biomater 9, 9243 (2013)

25. Y. Gao, X. Zou, J.X. Zhao, Y. Li, X. Su, Colloid. Surface. B 112, 128 (2013)

26. K. Liu, J.J. Zhang, F.F. Cheng, T.T. Zheng, C. Wang, J.J. Zhu, J. Mater. Chem 21, 12034 (2011)

27. H. Rouhi Saadabad, B. Akhlaghinia, J. Braz. Chem. Soc 25, 253 (2014)

669 28. X. Ling, Y. Xie, X. Lin, L. Li, T. Qiu, Chinese. J. Chem. Eng 27 (2019)
670
671
672 29. M. Khosravi, S. Arabi, Water. Sci. Technol. 74, 343 (2016)
673
674 30. M.K. Akalın, K. Tekin, M. Akyüz, S. Karagöz, Ind. Crop. Prod 76,829 (2015)
675
676 31. T. Liu, K. Wang, M. Jiang, L. Wan, Colloid. Surface. B 180, 221 (2019)
677
678 32. N. Pan, Y. Wang, X. Ren, T.S. Huang, I. Soo Kim, Mater. Sci. Eng. C. Mater. Biol. Appl
679 103, 19887 (2019)
680
681 33. I. Langmuir, J. Am. Chem. Soc 40, 1361 (1918)
682
683 34. H. Frendlich, J. Phys. Chem 57, 385 (1906)
684
685 35. M. Temkin, V. Phyzev, Acta. Physicochim. Urs 12, 217 (1940)
686
687 36. M.M. Dubinin, Chem. Rev 60, 235 (1960)
688
689 37. A.B. Albadarin, M. Charara, B.M.A. Tarboush, M.N.M. Ahmad, T.A. Kurniawan, N. Mu,
690 J. Mol. Liq 242, 478 (2017)
691
692 38. F. Siami, H. Ahmad panahi, A. Heidarinasab, E. Moniri, A. Akbarzadeh, H. Ebrahimi
693 Shahmabadi, Int. J. Med. Res. Health. Sci 5, 88 (2016)
694
695 39. Z. Berizi, S.Y. Hashemi, M. Hadi, A. Azari, A.H. Mahvi, Water. Sci. Technol 74, 1235
696 (2016)
697
698 40. D. Wójcik-Pastuszka, J. Krzak, B. Macikowski, R. Berkowski, B. Osiński, W. Musiał,
699 Materials 12, 1202 (2019)
700
701 41. A. Agrawal, R. Purwar, Indian. J. Fibre. Text 43, 104 (2018)
702
703 42. L. Pourtalebi Jahromi, M. Ghazali, H. Ashrafi, A. Azadi, Heliyon 6, 03451 (2020)
704
705 43. R. Gouda, H. Baishya, Z. Qing, J. Develop. Drugs 6 (2017)

44. K. A. Gates , H. Grad, P. Birek, P.I. Lee, Pharm. Res 11, 1605 (1994)

45. A. A. Elzatahry, M. S. Mohy Eldin, Polym. Adv. Technol 19, 1787 (2008)

46. S. Latha, P. Selvamani, C. Senthil Kumar, P. Sharavanan, G. Suganya, V. Singh Beniwal, P. Rama Rao, J. Magn. Magn. Mater 321, 1580 (2009)

47. D.J. Yang, C.D. Xiong, T. Govender, Y.Z. Wang, J. Biomater. Sci. Polym. Ed 20, 1321 (2009)

Supporting Information

Additional supporting information may be found online in the Supplementary Material section at the end of the article.

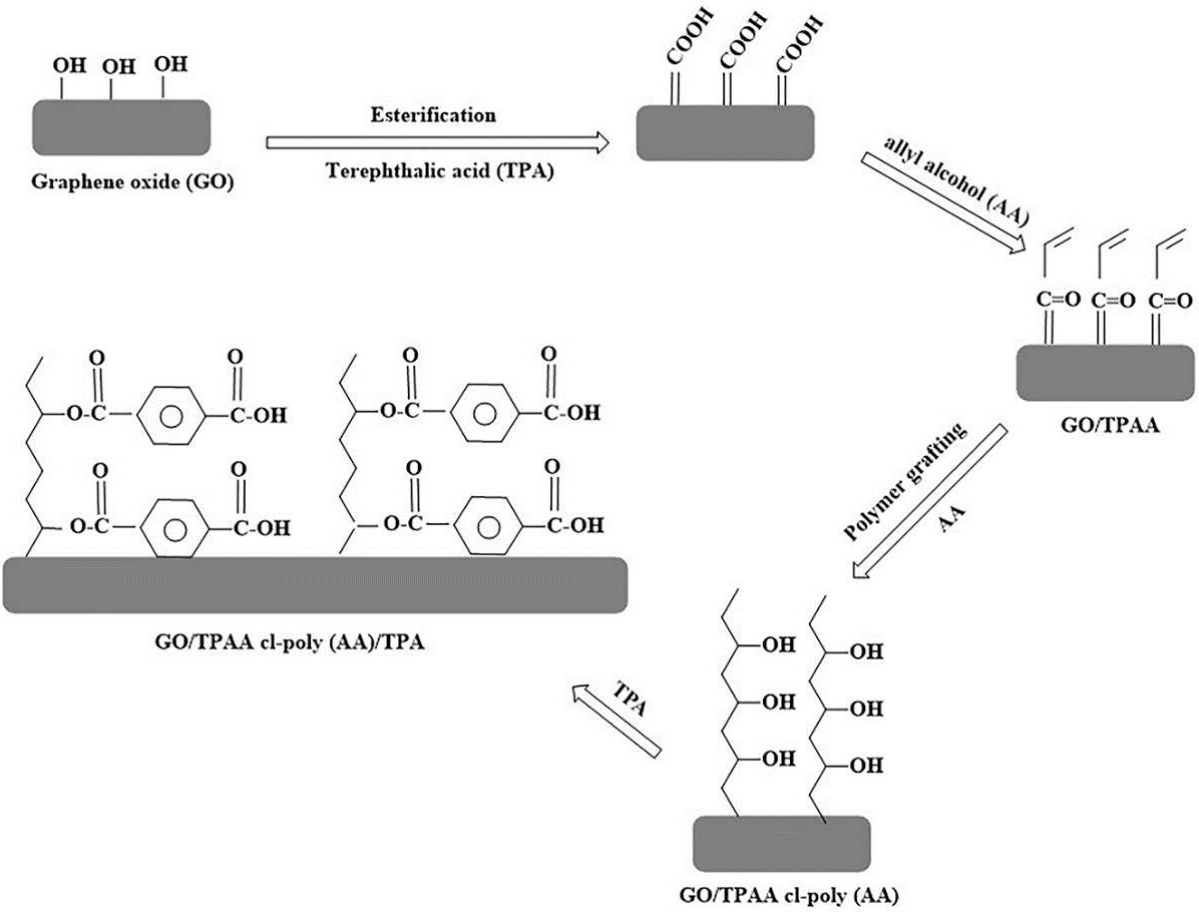

735

736 **Fig.1.** Schematic representation of preparation of GO/TPAA cl-poly (AA)/TPA.

737

738

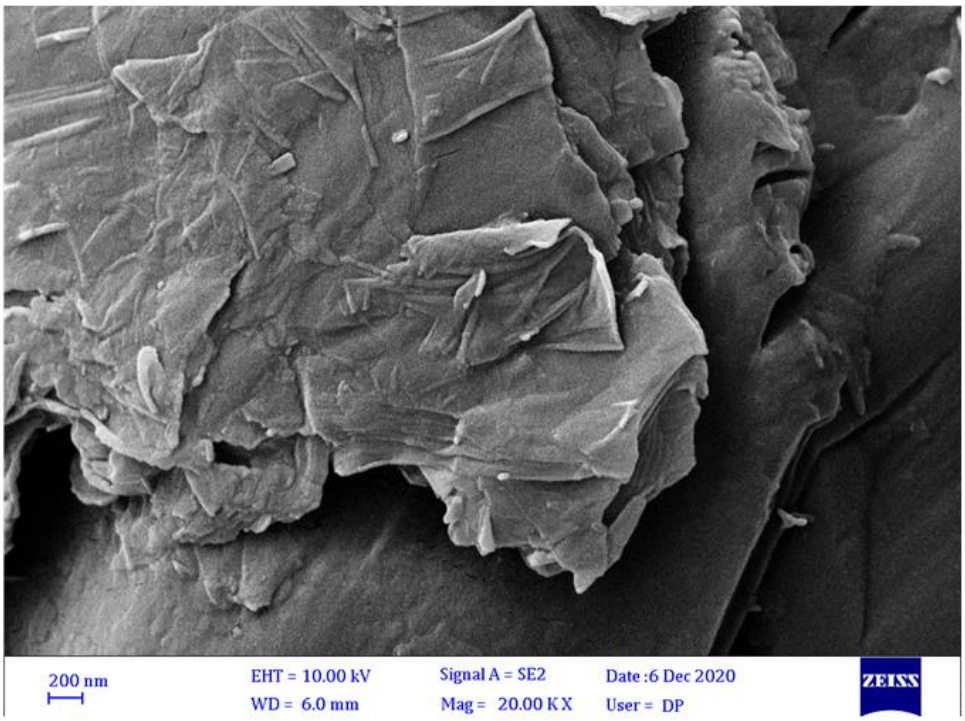
200 nm
EHT = 10.00 kV
WD = 6.0 mm
Signal A = SE2
Mag = 20.00 K X
Date :6 Dec 2020
User = DP
ZEISS

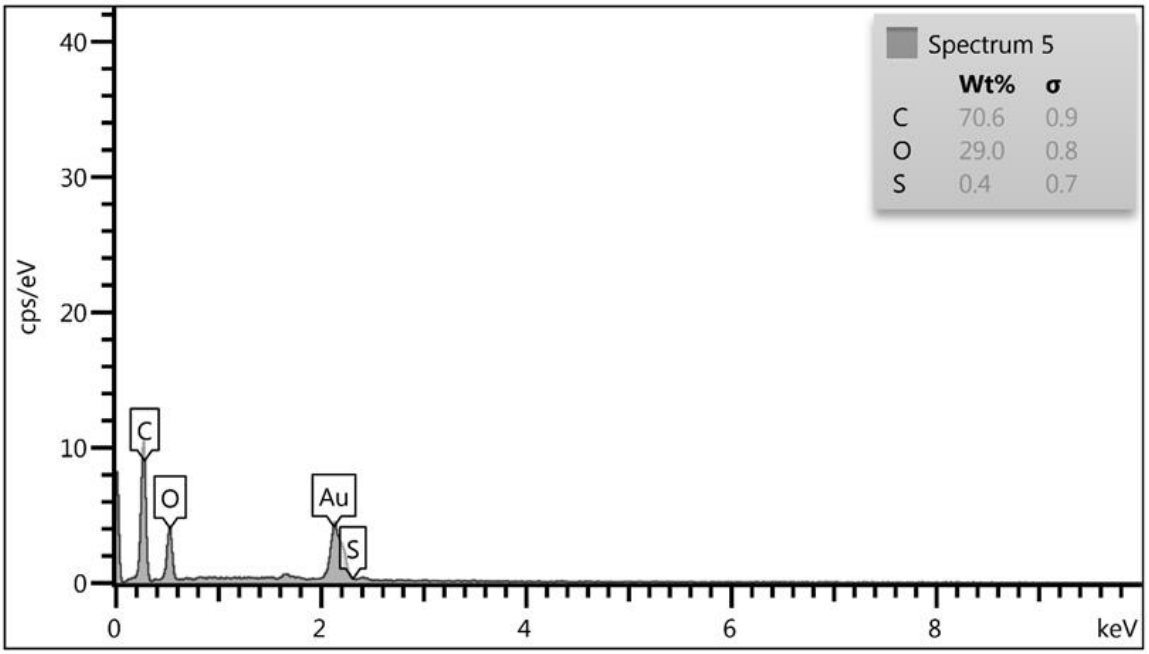
Spectrum 5
Wt% σ
C 70.6 0.9
O 29.0 0.8
S 0.4 0.7
cps/eV
40
30
20
10
0
C
O
Au
S
0
2
4
6
8
keV

(a)

739

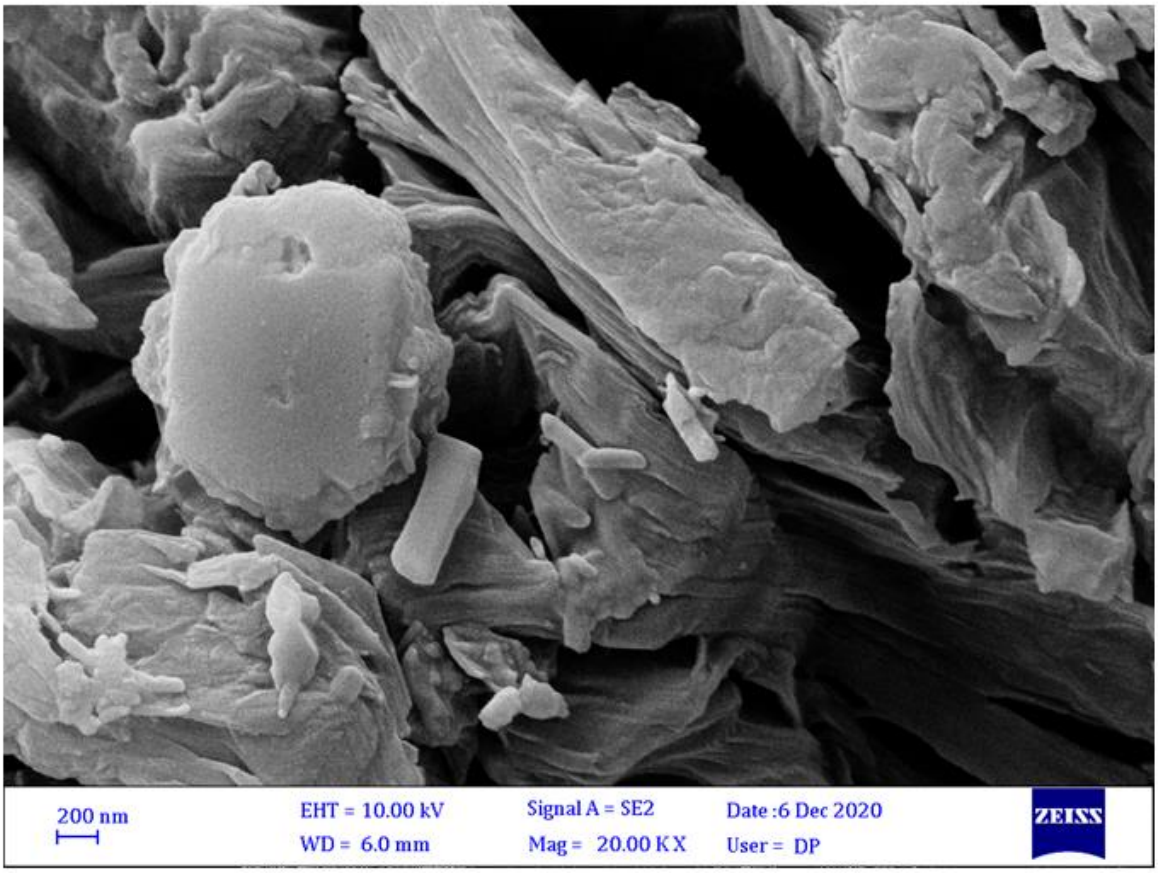
200 nm
EHT = 10.00 kV
WD = 6.0 mm
Signal A = SE2
Mag = 20.00 K X
Date :6 Dec 2020
User = DP
ZEISS

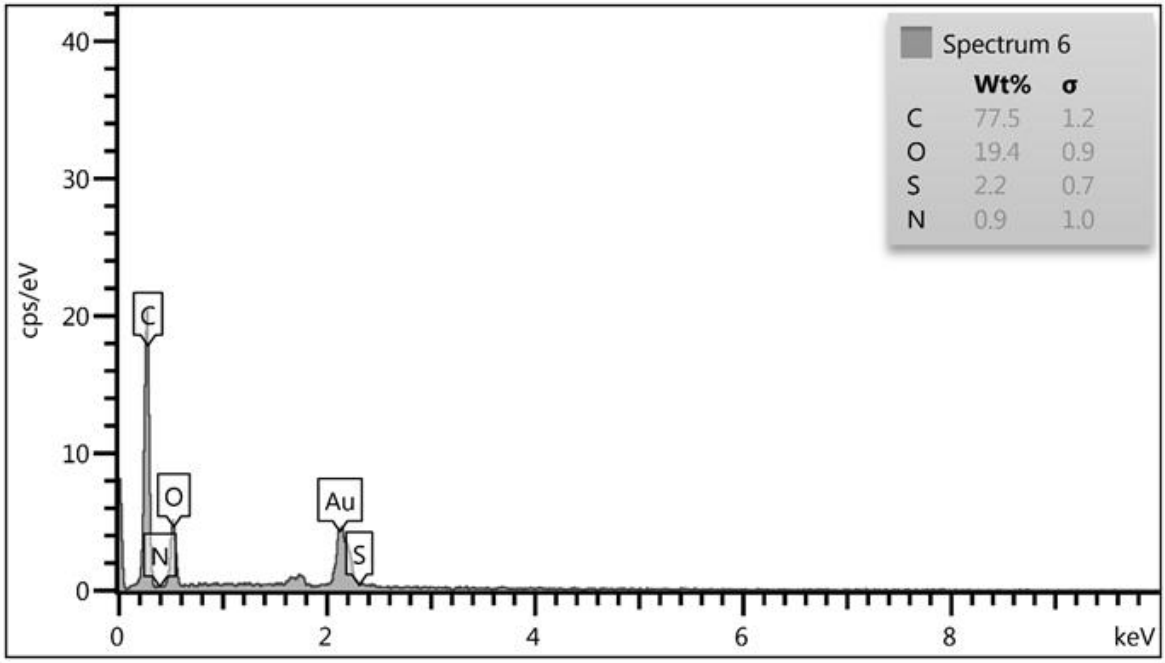
Spectrum 6
Wt% σ
C 77.5 1.2
O 19.4 0.9
S 2.2 0.7
N 0.9 1.0
cps/eV
40
30
20
10
0
C
O
N
Au
S
0
2
4
6
8
keV

(b)

740

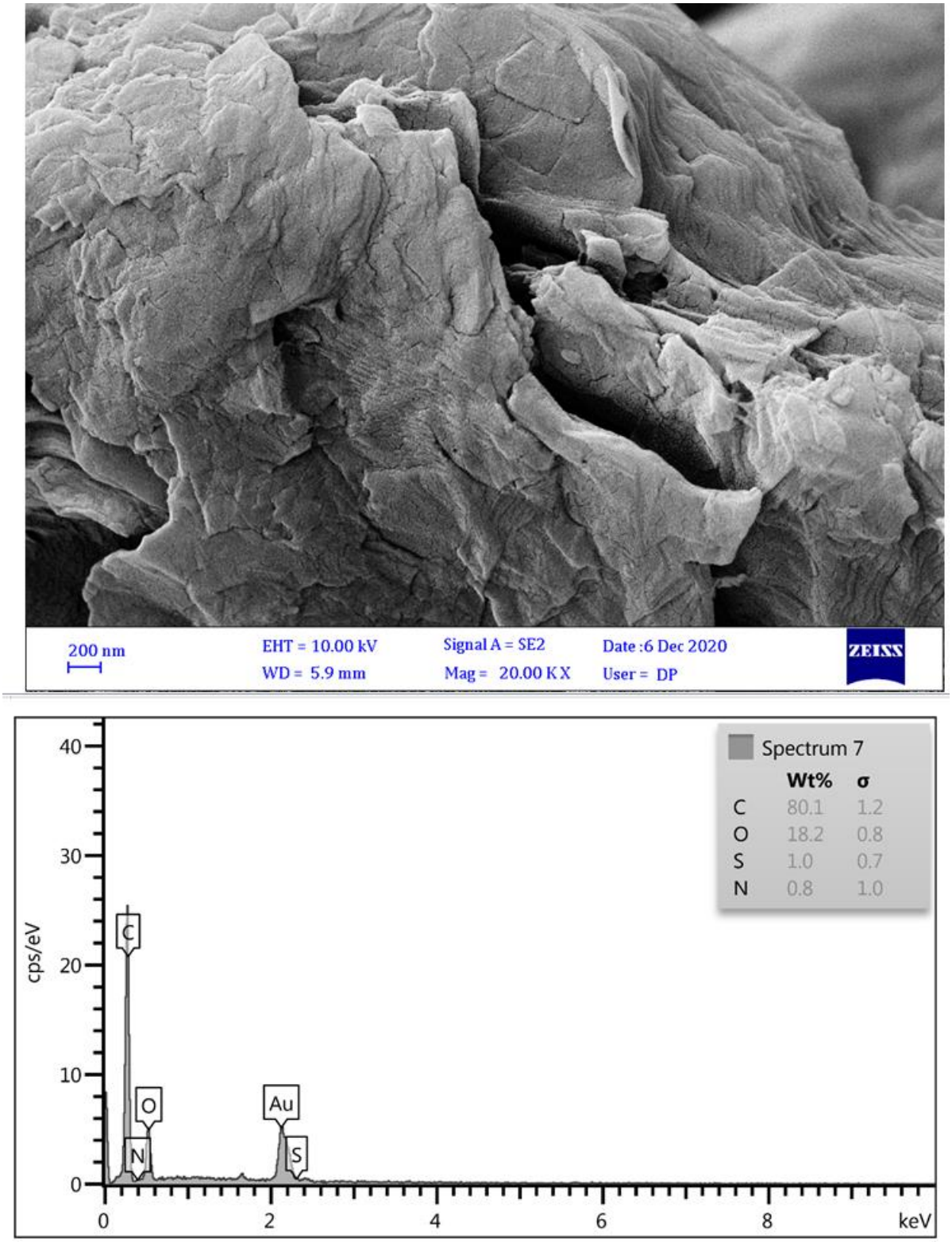

(c)

Fig.2. SEM and EDX images of (a) GO/TPAA, (b) GO/TPAA cl-poly (AA), and (c) GO/TPAA cl-poly (AA)/TPA.

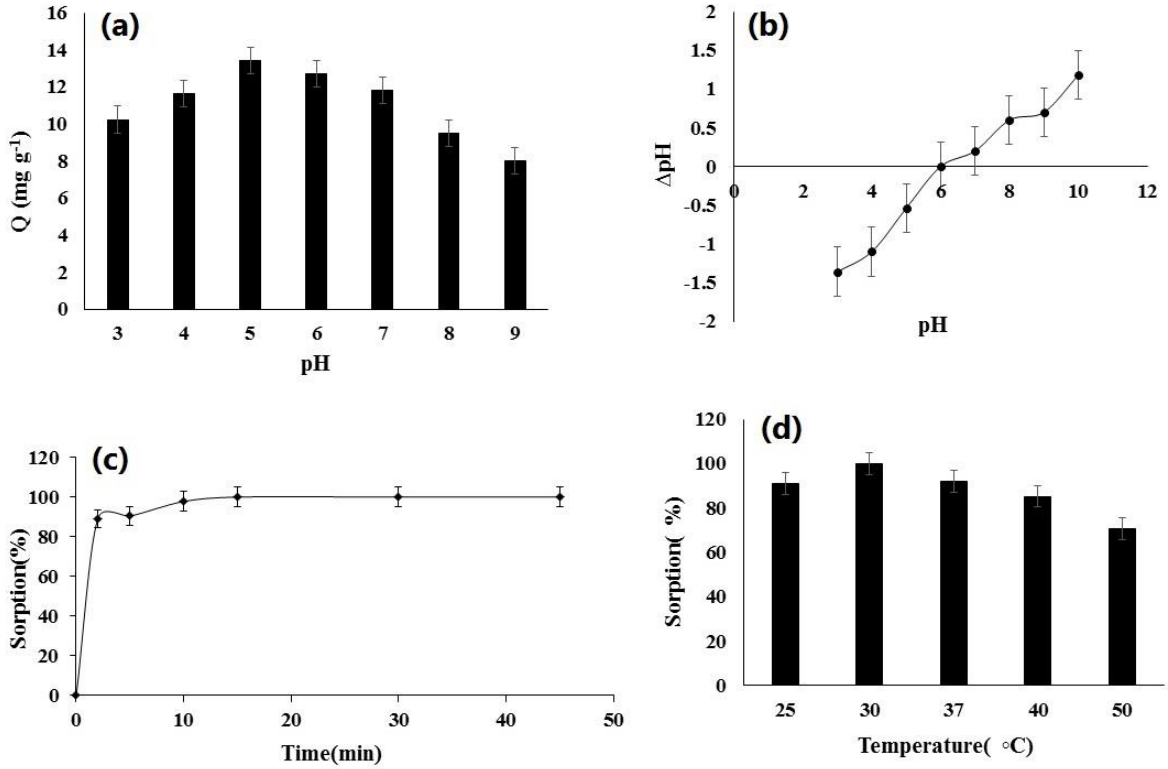

745

746

747 **Fig.3.** The influence of pH (a), pH $_{PZC}$ (b), contact time (c) and temperature (d) on the

748 sorption of MNZ onto GO/TPAA cl-poly (AA)/TPA.

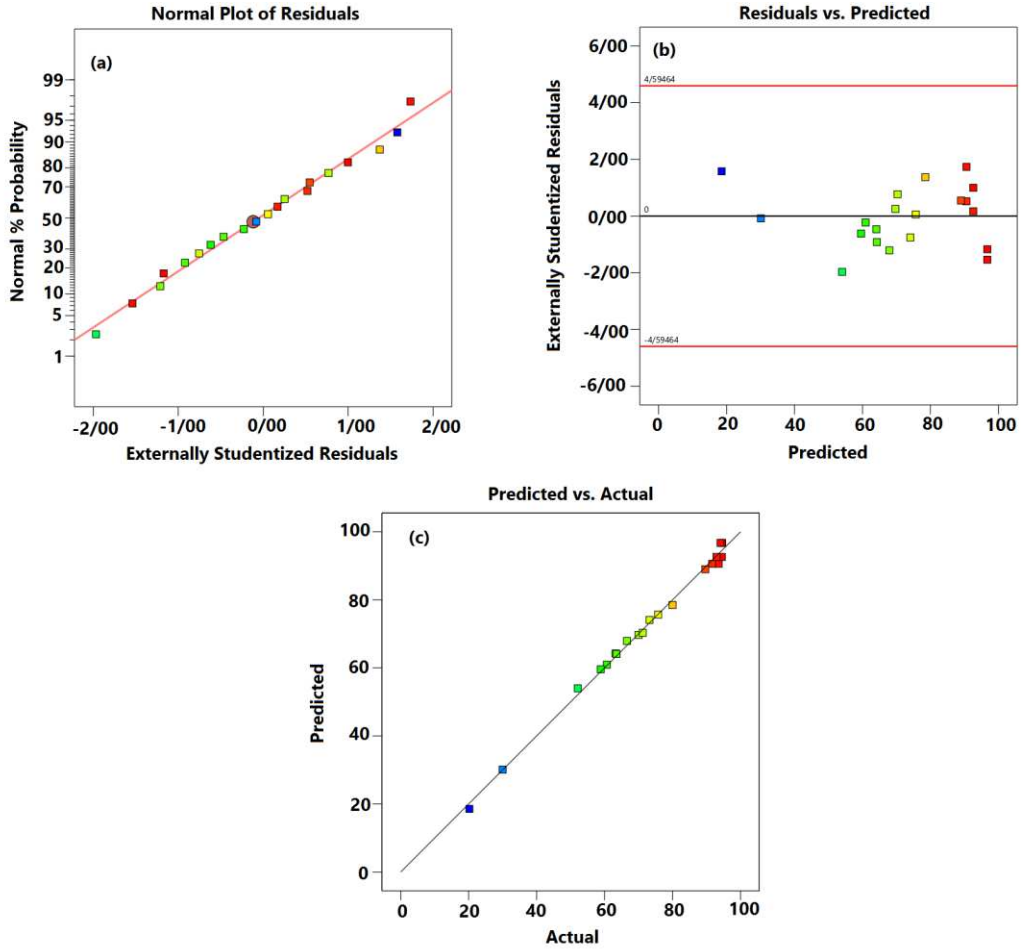

Fig. 4. (a) Normal plot of residuals, (b) plot of residuals versus predicted, and (c) plot of predicted values versus actual values related to the adsorption of the drug

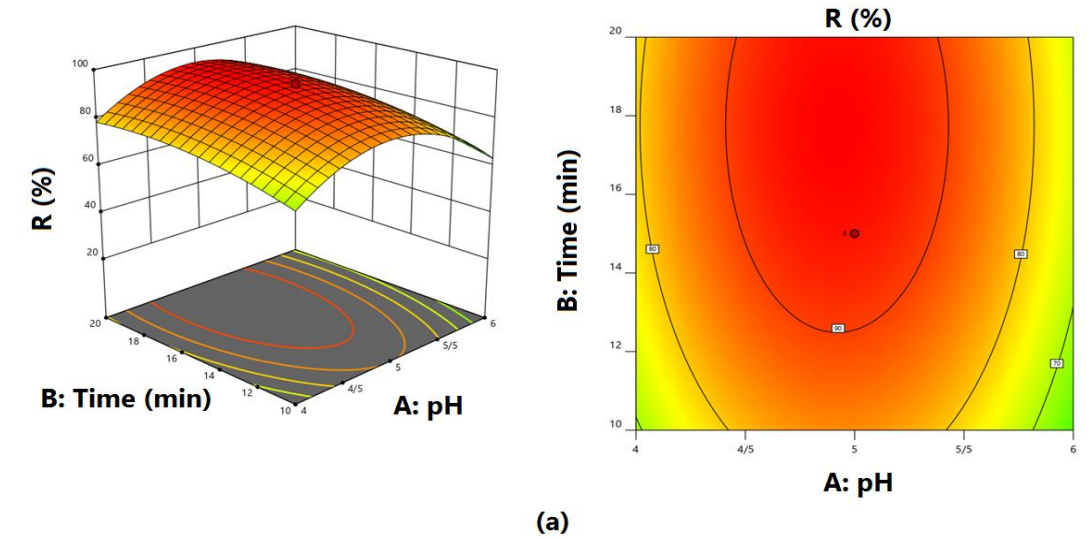

(a)

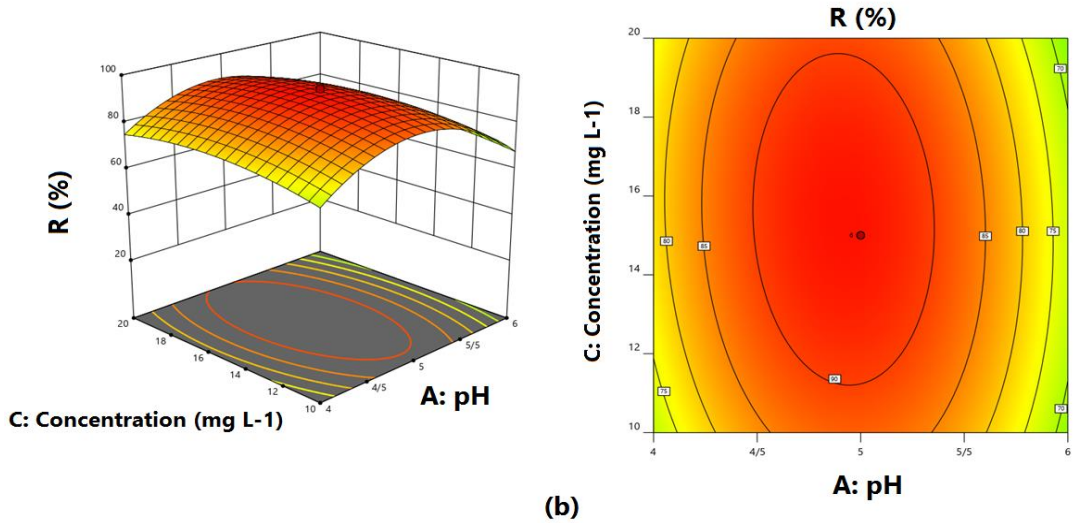

(b)

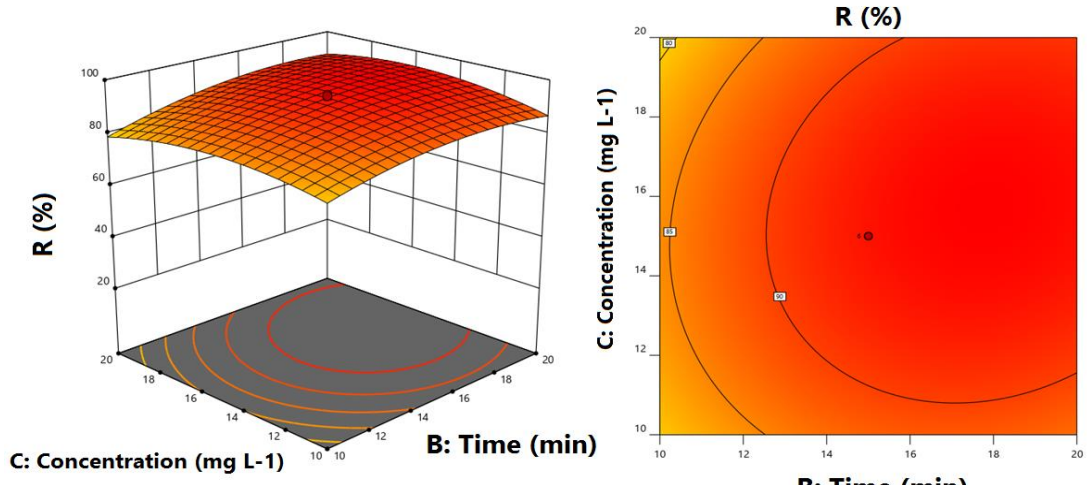

(c)

Fig.5. Response surface and contour plots for the adsorption efficiency of MNZ: (a) pH and contact time; (b) pH and concentration; (c) time and concentration.

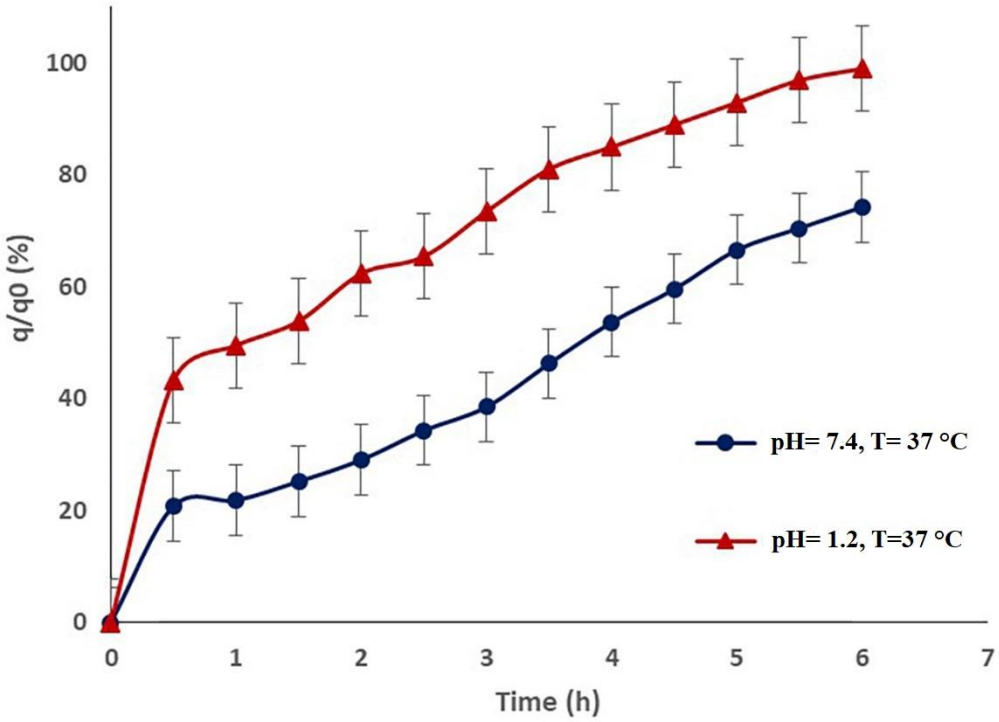

Fig.6. Drug release behavior in stimulated intestinal fluid and in stimulated gastric fluid.

Supplementary Files

This is a list of supplementary files associated with this preprint. Click to download.

- SupplementaryS.docx